

Route to chaos for combustion instability in ducted laminar premixed flames

Lipika Kabiraj, Aditya Saurabh, Pankaj Wahi, and R. I. Sujith

Citation: [Chaos](#) **22**, 023129 (2012);

View online: <https://doi.org/10.1063/1.4718725>

View Table of Contents: <http://aip.scitation.org/toc/cha/22/2>

Published by the [American Institute of Physics](#)

Articles you may be interested in

[Chaos in an imperfectly premixed model combustor](#)

[Chaos: An Interdisciplinary Journal of Nonlinear Science](#) **25**, 023101 (2015); 10.1063/1.4906943

[Characterization of complexities in combustion instability in a lean premixed gas-turbine model combustor](#)

[Chaos: An Interdisciplinary Journal of Nonlinear Science](#) **22**, 043128 (2012); 10.1063/1.4766589

[Dynamic properties of combustion instability in a lean premixed gas-turbine combustor](#)

[Chaos: An Interdisciplinary Journal of Nonlinear Science](#) **21**, 013124 (2011); 10.1063/1.3563577

[Dynamics of self-excited thermoacoustic instability in a combustion system: Pseudo-periodic and high-dimensional nature](#)

[Chaos: An Interdisciplinary Journal of Nonlinear Science](#) **25**, 043107 (2015); 10.1063/1.4914358

[Change of criticality in a prototypical thermoacoustic system](#)

[Chaos: An Interdisciplinary Journal of Nonlinear Science](#) **27**, 023106 (2017); 10.1063/1.4975822

[Network structure of turbulent premixed flames](#)

[Chaos: An Interdisciplinary Journal of Nonlinear Science](#) **27**, 043107 (2017); 10.1063/1.4980135

Welcome to a

Smarter Search



PHYSICS
TODAY

with the redesigned
Physics Today Buyer's Guide

Find the tools you're looking for today!

Route to chaos for combustion instability in ducted laminar premixed flames

Lipika Kabiraj,^{1,a)} Aditya Saurabh,^{1,b)} Pankaj Wahi,² and R. I. Sujith¹

¹Department of Aerospace Engineering, Indian Institute of Technology Madras, Chennai 600036, India

²Department of Mechanical Engineering, Indian Institute of Technology Kanpur, Kanpur 208016, India

(Received 7 September 2011; accepted 30 April 2012; published online 23 May 2012)

Complex thermoacoustic oscillations are observed experimentally in a simple laboratory combustor that burns lean premixed fuel-air mixture, as a result of nonlinear interaction between the acoustic field and the combustion processes. The application of nonlinear time series analysis, particularly techniques based on phase space reconstruction from acquired pressure data, reveals rich dynamical behavior and the existence of several complex states. A route to chaos for thermoacoustic instability is established experimentally for the first time. We show that, as the location of the heat source is gradually varied, self-excited periodic thermoacoustic oscillations undergo transition to chaos via the Ruelle-Takens scenario. © 2012 American Institute of Physics.

[<http://dx.doi.org/10.1063/1.4718725>]

Combustion-driven thermoacoustic oscillations that can emerge spontaneously in combustion systems, in the form of self-sustained pressure and heat release rate oscillations, are detrimental to the system and are a hindrance to the development of clean combustion technology, due to the problem of inherent instability associate with premixed flame. To understand the phenomenon, it is particularly important to know the nonlinear aspects of the self-excited oscillations. In this paper, we investigate the nonlinear characteristics of thermoacoustic oscillations in a model thermoacoustic system, through experimental bifurcation analysis. By changing a control parameter, the location of the source of combustion, we observe that oscillations are spontaneously excited and subsequently undergo qualitative changes in their dynamical behavior as the location is further varied. The transition to self-excited, limit cycle oscillations is shown to occur via the subcritical Hopf bifurcation. Following this transition, we observed that the system enters a chaotic state via a quasi-periodic route (the Ruelle-Takens scenario), which has also been observed in several other physically observed nonlinear systems. We incorporate techniques from advanced nonlinear time series analysis for investigating the dynamics of these oscillations and to identify the route to chaos. The results indicate the importance of studying thermoacoustic instability from the point of view of dynamical systems theory.

I. INTRODUCTION

Complex nonlinear behaviors such as quasi-periodicity and chaotic oscillations have been reported for forced response of acoustic¹ and combustion systems^{2,3} and Taconis oscillations in a gas column driven by temperature gradient.⁴

^{a)}Author to whom correspondence should be addressed. Electronic mail: lipikakabiraj@gmail.com.

^{b)}Present address: Chair of Fluid Dynamics, Hermann-Föttinger-Institut, Technische Universität Berlin, Müller-Breslau Str. 8, Berlin 10623, Germany.

Observations of such complex behaviors of self-excited oscillations in combustion-driven thermoacoustic systems such as those found in industrial gas turbines, furnaces, and other practical combustion applications, although reported by a few researchers, have not been investigated in detail. Hence, there is a need to further investigate the nonlinear aspects of combustion oscillations for the development of combustion systems.

Self-excited combustion instabilities that arise due to combustion-acoustic interactions are a serious engineering problem. These are known to cause dangerous pressure and heat release rate oscillations in practical combustion systems such as rocket motors, jet engines, and gas-turbine engines. These oscillations cause increased mechanical and thermal loading on structures along with increased pollutant gas emissions in practical combustion systems. Thus, combustion instability has adverse effects on the efficiency, safe operating range, and life-span of the system and hence its investigation is of great interest to the propulsion and power industry.

Combustion instability is an interplay of several phenomena—combustion, acoustics, and hydrodynamics being the major processes. Hence, it is quite complex to predict and model for even simple configurations. Stating briefly, the unsteady heat release rate gives rise to pressure and velocity fluctuations. These acoustic fluctuations again interact with the flame and this flame-acoustic interaction then leads to amplification in the perturbation amplitudes of acoustic fluctuations and heat release rate. Under certain conditions determined by the time scales associated with combustion, acoustics, and hydrodynamics within the duct, this could result in the development of a positive feedback loop where pressure and heat release rate oscillations grow exponentially. When these oscillations attain a large enough amplitude, nonlinear mechanisms, for instance, the saturation of heat release rate, come into picture.⁶ The asymptotic state of the instability is governed by nonlinear processes and therefore may require special techniques for investigation.

Complex thermoacoustic oscillations have been reported previously, in literature, by a few authors. Jahnke and Culick⁸ have reported the possibility of quasi-periodic thermoacoustic oscillations through their numerical continuation analysis of a solid rocket motor. Sterling¹² and later Lei and Turan¹³ have reported chaotic oscillations through numerical bifurcation analysis of premixed combustors with different models for combustion processes. In experiments, Fichera *et al.*¹⁴ have reported chaotic dynamics of heat release rate fluctuations in a lean gas turbine combustor. Recently, Gotoda *et al.*² have presented an experimental investigation for transition of thermoacoustic oscillations from stochastic fluctuations to periodic oscillations through low dimensional chaotic oscillations, with respect to equivalence ratio changes.

Through experimental bifurcations analysis, we study the transition of periodic self-excited states to aperiodic oscillations in a ducted laminar premixed flame configuration. We perform this investigation in a relatively thermoacoustic system that consists of a simple multiple-flame burner enclosed in a duct. The configuration has the advantage that the properties of combustion instability can be studied without significant interference from hydrodynamic instability. In addition, the dynamics of laminar flames exposed to acoustic perturbations has been extensively studied through experiments¹⁵ and numerical investigations.¹⁶ This makes the configuration ideal for fundamental studies on self-excited combustion instability.

In this paper, we investigate the phenomena of combustion instability in the light of nonlinear dynamics. The implementation of advanced nonlinear time series analysis techniques,¹⁸ yields new insight into the dynamics of thermoacoustic oscillations. The experimentally acquired data in terms of pressure and heat release rate oscillations were characterized by the application of nonlinear time series analysis techniques.¹⁸

Presently, combustion instability, also known as thermoacoustic instability, is associated synonymously with limit cycle oscillations.⁵ The results obtained in this investigation indicate that thermoacoustic systems can display rich dynamical behavior. We show the presence of chaotic and several other complex self-excited oscillation states in a combustion driven thermoacoustic system. The route to chaos followed by our system is identified to be a quasi-periodic transition, which has also been observed in Rayleigh-Bénard convection experiments.¹⁹ Although chaos has been observed in self excited combustion driven oscillations, the route to chaos has not been identified experimentally to date.

The paper is divided into following sections: We start the discussion by first introducing the experimental setup and the instrumentation employed for this study (Sec. II). In Sec. III, we discuss the results obtained from the bifurcation analysis of the system in the light of dynamical systems theory. Discussion on the nonlinear time series analysis techniques utilised for data analysis is presented in Sec. III A. Finally, we discuss on the implication of our findings in Sec. IV and state our concluding remarks in Sec. V.

II. EXPERIMENTAL SETUP

A schematic of the experimental setup is given in Fig. 1. A steel tube of inner diameter 16 mm, thickness 1.5 mm, and length 800 mm is used as the burner tube. The tube is connected to a large cylindrical decoupling chamber. This chamber decouples the downstream acoustics and fluctuations in the fuel and air supply system. The fuel, liquefied petroleum gas (LPG), and air are mixed further upstream in a premixing chamber stuffed with steel wool for enhanced mixing of the gases. On the burner tube, a perforated copper block, 18 mm in height, with seven holes of diameter 2 mm is mounted. Seven small conical flames stabilise on this copper block. A fine wire mesh is installed on top of the perforated copper block to prevent flame blow-off during the instability. This configuration is similar to the multiple injection configuration used by Matsui²⁰ and more recently by Noiray *et al.*,¹⁶ for flame transfer function measurements. The burner is enclosed within a transparent borosilicate glass duct of inner diameter 56.7 mm. The glass duct is closed at the bottom, providing an acoustically rigid boundary condition. The top end is open to the atmosphere. The glass duct is connected to a traverse system which is used to translate the duct on the burner tube in the vertical direction, thereby changing the location of the multiple flames with respect to the duct. The relative flame location can be measured with an uncertainty of $\pm 1\text{ mm}$.

Experiments were conducted at an equivalence ratio of $\phi = 0.48$, by keeping the volumetric fuel flow rate at 60 ccm and the volumetric air flow rate at 4 lpm, measured using rotameters with a maximum error corresponding to 2% of the rotameter full scale readings. The corresponding uncertainty in the equivalence ratio is estimated to be 2.8%. In

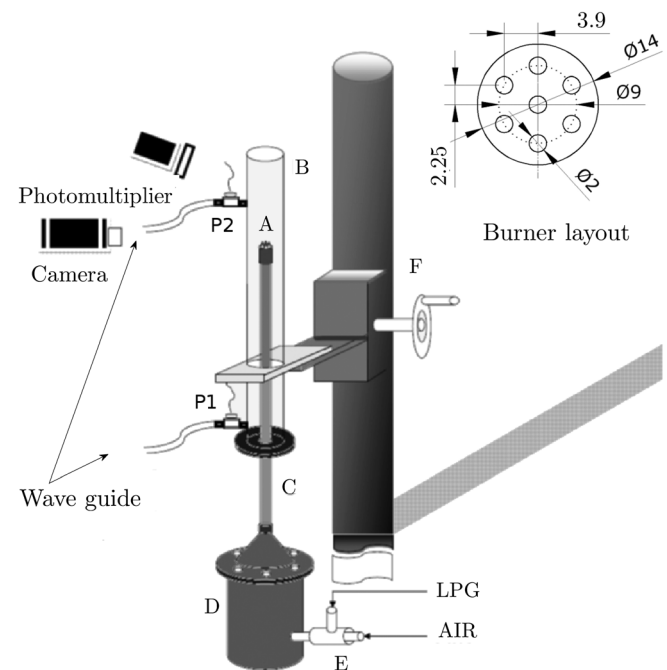


FIG. 1. Schematic of the thermoacoustic setup, A—premixed flames, B—open-closed, transparent borosilicate glass duct, C—burner tube, D—decoupler, E—LPG-air premixer, F—traverse, P1 and P2—pressure sensors. A top view of the burner is given at the top right corner of the figure; all dimensions are in mm.

practical applications, lean-premixed combustion is preferred over combustion of rich fuel-air mixtures due to lower pollutant emission. Unfortunately, systems running on lean-premixed combustion are more susceptible to combustion instability. Hence, this configuration is of particular importance to aerospace applications. Therefore, for this investigation, we also choose a lean equivalence ratio.

Data acquisition consists of measurement of pressure fluctuations within the duct and flame intensity fluctuations. Two pressure microphones (model number 103B02, PCB piezotronics make), P1 and P2, mounted on the walls of the glass duct were used to measure pressure oscillations at positions shown by P1 and P2 in Fig. 1. The pressure time series (p) used for the analysis in this paper were obtained from the microphone mounted near the close end of the glass duct P1, at a distance of 50 mm from the bottom of the glass duct. Pressure fluctuations due to standing waves in the duct are always maximum near the acoustically rigid end and, hence, the signal-to-noise ratio will be higher for pressure signals acquired by microphone P1. As mentioned already, thermoacoustic oscillations occur due to a positive feedback between pressure fluctuations and unsteady heat release rate. Therefore, along with pressure oscillations, it is also important to capture heat release rate oscillations. Since CH radical emission (chemiluminescence measurements $I(t)$) is known to be proportional to heat release rate from premixed flames,²¹ time series of CH radical emission has been acquired using a photomultiplier tube (model number H5784, Hamamatsu) equipped with a narrowband CH radical filter (bandwidth 10 nm, centered at 431.4 nm), simultaneously with pressure oscillations. A 16-bit analog to digital conversion card (NI-6143) was used for data acquisition which has a resolution of 0.15 mV, considering the input voltage range to be ± 5 V. The uncertainty in pressure microphone measurement is ± 0.14 Pa.

The exponential decay rate of the system, determined at cold flow conditions prior to the experiments, was obtained to be 16/s, using an acoustic pulse introduced in the system. Experiments are performed only if the decay rate is within $\pm 10\%$ of the stated value. Thus, acoustic damping is maintained within bounds to ensure repeatability of the experiments.

III. RESULTS

As we gradually change the flame location, the system goes from a steady state to a self-excited oscillatory state. From the point of the onset of thermoacoustic instability, if the flame location is varied further, properties of the self-excited state change dramatically. In order to track the changes in oscillations with respect to the flame location, we plot an orbit/bifurcation diagram (Fig. 2). Corresponding to every flame location (x_f), we plot the amplitudes of the local maxima²² in the acquired pressure time series for that particular x_f . The number of local maxima, at a given parameter, gives the period of oscillations: a single local maxima indicates a limit cycle oscillation, two local maxima values suggest period two oscillations and so on. The Roman numerals (I-VIII) are used to indicate different

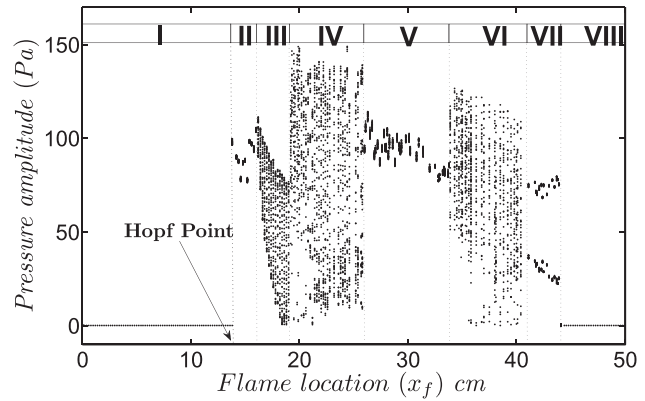


FIG. 2. Bifurcation plot summarising the experiment: Hopf point at $x_f = 13.8$ cm. The Roman numerals (I-VIII) are used to indicate different regions in the bifurcation plot. Region I—steady state and region VIII—steady state.

regions in the bifurcation plot. Time series and frequency spectra for oscillations in these regions are presented in Fig. 3. A longer time window is used for more complicated oscillations so that the essential features of the oscillations are clearly depicted.

The onset of instability occurs at $x_f = 13.8$ cm, one-eighth of the total duct length from the open end. At this point, there is a qualitative change in the system from steady state to finite amplitude oscillations. This is an indication of a subcritical Hopf bifurcation.²² It is quite common to encounter subcritical Hopf bifurcation in practical combustion-driven thermoacoustic systems such as gas-turbine combustors and rocket combustors.⁵ The point at which the bifurcation occurs is referred to as the Hopf point. The bifurcation results in a single frequency, “limit cycle” oscillation with a frequency $f \sim 570$ Hz. This is close to the second harmonic of the duct acoustic mode. The time series and frequency spectrum of this state are shown in Figs. 3(IIa) and 3(IIb), respectively.

The limit cycle oscillation state persists for a small range of x_f values beyond which it is followed by a bifurcation of the limit cycle to another type of oscillation with more than one dominating frequency ($f_1 \sim 570$ Hz, $f_2 \sim 364.1$ Hz), as shown in Fig. 3(IIIa). As we change the flame location, the frequencies compete with each other and eventually towards the end of this state, the time series (Fig. 3(IIIa)) and the frequency spectrum (Fig. 3(IIIb)) changes to the one depicted in Figs. 3(IIIc) and 3(IIId), respectively. The dominant frequency also changes from f_1 to f_2 , which is close to the first harmonic duct acoustic mode.

The next bifurcation occurs at $x_f = 19.2$ cm, the amplitude of local maxima increases to about 1.5 times (150 Pa). The irregularity in the oscillations can be clearly seen in Fig. 3(IVa). The corresponding frequency spectrum, Fig. 3(IVb), shows the presence of a broad band of frequencies (along with the appearance of a new independent frequency, $f_3 \sim 524$ Hz) suggesting the presence of low dimensional chaos. On changing the flame location, we observe that the signature of the time series has changes at $x_f = 21$ cm, within region IV. We observe regularity in the time series and distinct peaks in the frequency spectrum plots (Figs.

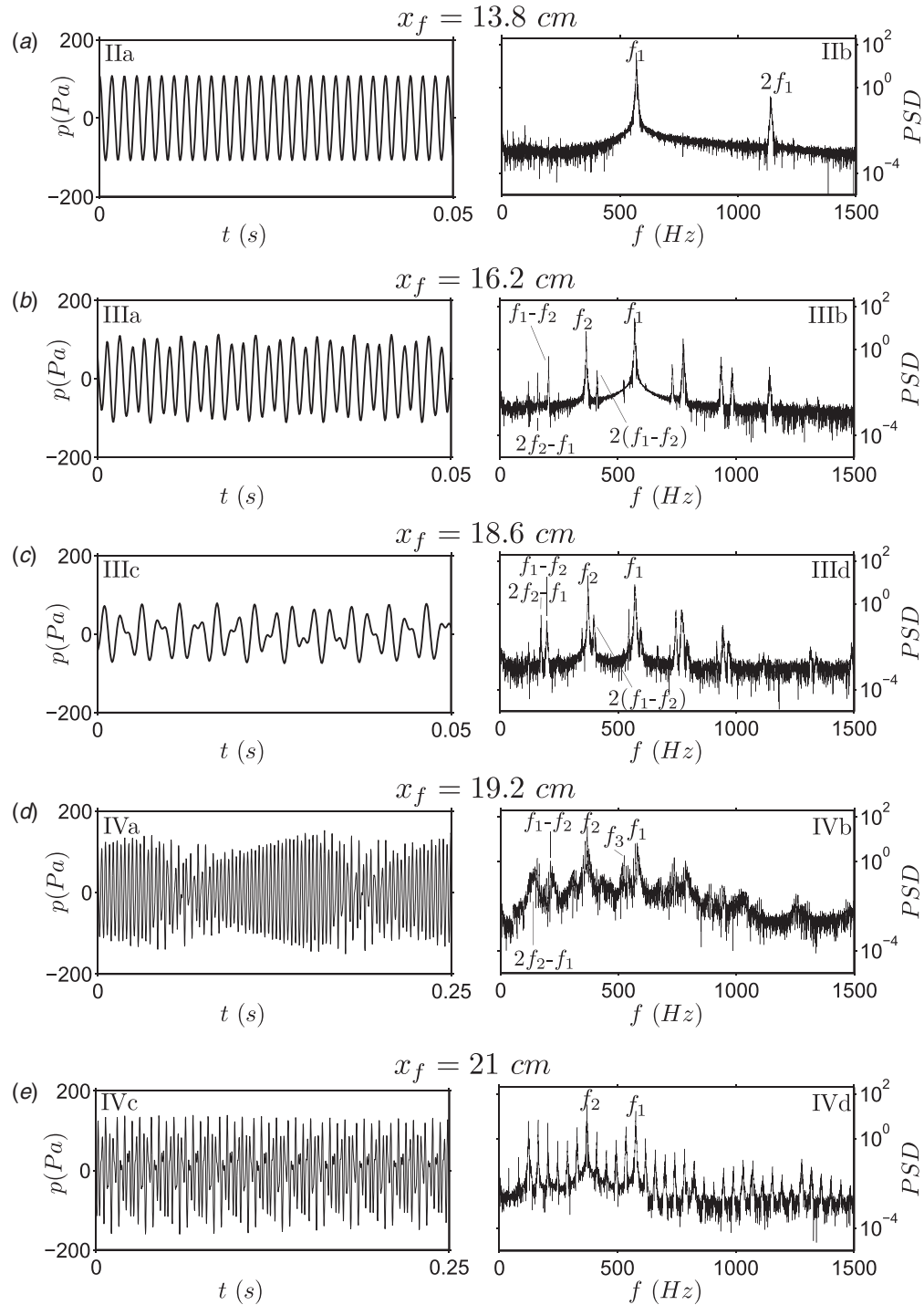


FIG. 3. Time series and power spectrum for various oscillating states observed in the system, labelled according to the bifurcation plot, Fig. 2.

3(IVc) and 3(IVd)). The frequencies in the spectrum are rationally related as opposed to the broadband frequencies. Following this state, the oscillations become regular again in region V.

Figures 3(Va) and 3(Vb) show the time series and frequency spectrum plots of a representative state in region V (Fig. 2). The peaks in the frequency spectrum correspond to f_2 , $f_2/2$, and $f_2/4$. This is an indication of the oscillations being period four in nature, but since the contribution from the sub-harmonics is very less compared to the dominant frequency, it is not clearly visible in the time series or in the

bifurcation plot (Fig. 2). The system exists in this state for a large range of x_f values ($x_f = 25.8$ cm to $x_f = 33.9$ cm) and is followed by another state similar to the state corresponding to Fig. 3(IVa), as depicted in Figs. 3(VIa) and 3(VIb). The frequency spectrum shows three broadband regions centered around 553 Hz, 370.2 Hz, and 185.1 Hz, where 185.1 Hz is the sub-harmonic of 370.2 Hz. We increase the flame location further and this state changes to a period two oscillation in region VII (Fig. 2) via an intermittent state. The time series and frequency spectrum of the intermittent and the period two oscillatory state are given in Figs. 3(VIc), 3(VId) and

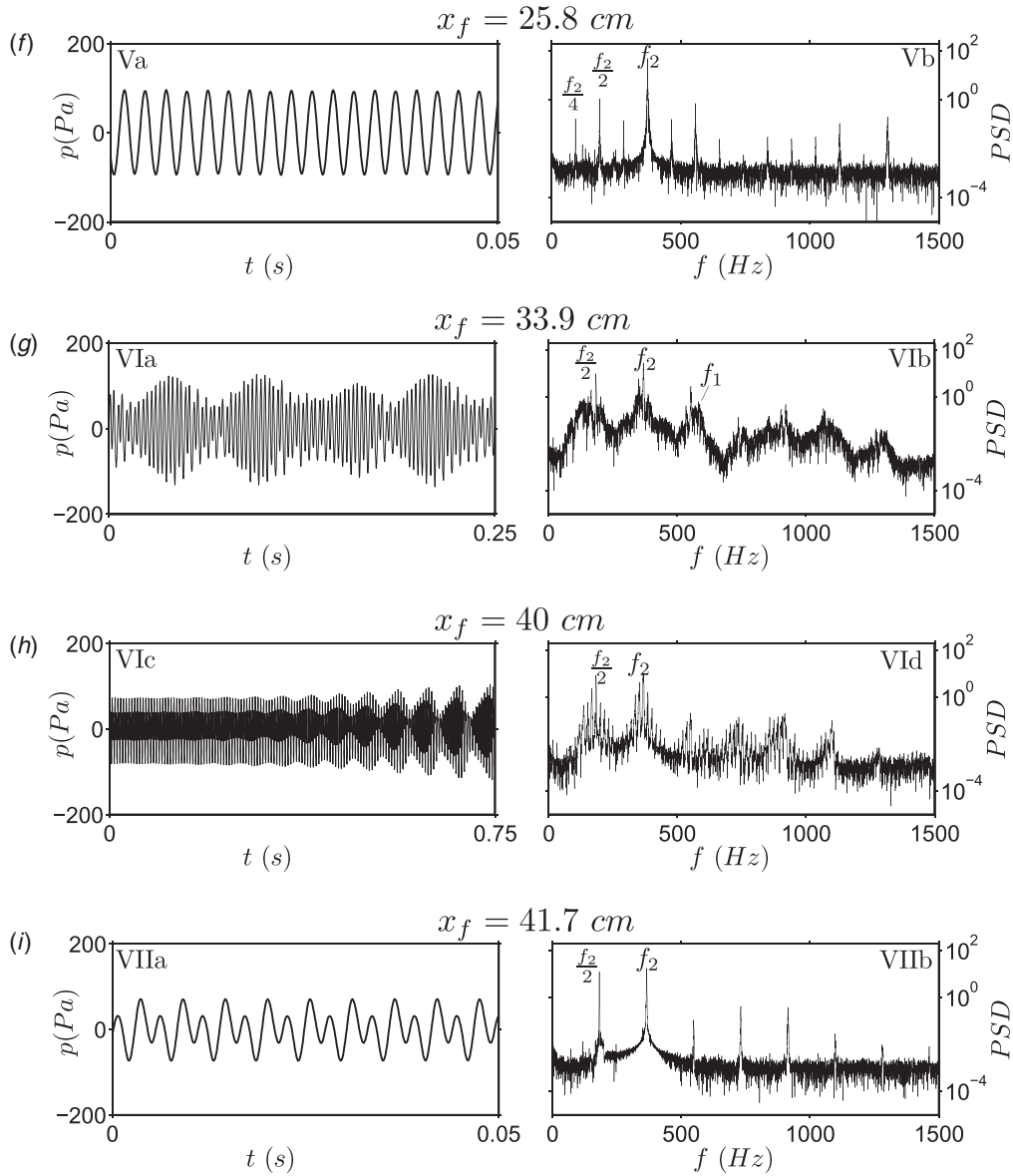


FIG. 3. Continued

3(VIIa), 3(VIIb), respectively. The intermittent state has intervals of period two and the irregular state coexisting together. A transition from period two to irregular oscillations can be observed in Fig. 3(VIc). Beyond this region, changing the flame location brings the system back to a steady state at $x_f = 43.9$ cm, which is close to half the duct length.

For further analysis, techniques that specifically deal with nonlinear systems are called for. It is crucial to implement nonlinear time series analysis techniques for understanding the dynamics of the thermoacoustic system. Nonlinear time series analysis techniques provide tools for systematic analysis and identification of characteristics and structures in time series data generated by nonlinear processes with emphasis on the determination of properties of a special class of nonlinear oscillations, the chaotic oscillations. Chaotic oscillations are quite commonly observed in nonlinear systems and in the absence of appropriate analysis could be misinterpreted as noise. Therefore, implementation of phase-space based nonlinear time series

analysis techniques is essential to extract detailed information about the complex nonlinear processes.

A. Nonlinear time series analysis

The most important step in the time series analysis technique used here is the representation of the asymptotic state of nonlinear oscillations in an appropriate phase space and investigation of the structure of the resulting attractor of system dynamics. This attractor is a mapping of the actual process in a finite dimensional space created from scalar observations. Topological measures of the so formed attractor, such as the correlation dimension and the Lyapunov exponents of the attractor can then be calculated. These quantities are direct measures of the complexity in the system. Developments in the theory of nonlinear time series analysis enable one to extract information on system dynamics based on scalar measurements obtained in experiments. Several nonlinear systems have been

successfully investigated in the light of these techniques and from this study, it can be seen that the nonlinear nature of thermoacoustic oscillations can also be studied through the application of these methods. The fundamental idea behind the time series analysis techniques employed in this work is given below.

1. Phase space reconstruction

Using the experimentally obtained time series data, we need to create a multi-dimensional space to reconstruct the time evolution of the dynamical system. A dynamical system is identified if all the state variables of the system including the required number of derivatives are known at all times. Several states of the system are generally related to each other through their derivatives and hence the state of the system can be represented in a state space created out of the derivatives of a single state of the system which has been measured. Since obtaining a proper representation of derivatives from discrete time series data is practically not possible, Takens²³ has demonstrated that a multivariate phase space constructed out of time-delayed coordinates extracted from the measured time series data can be used as an alternative. In the resulting coordinate system, the salient features of the orbits of the dynamical system are conserved. It is then possible to unfold the attractor of system dynamics in this space and to arrive at topological invariants of the system dynamics such as the attractor dimension and Lyapunov exponents.

The time-delayed coordinates from a time series data,^{24,34} $s(n) = s(t_0 + n\tau_s)$, where τ_s is the sampling time interval would be

$$y(n) = [s(n), s(n+T), s(n+2T), s(n+3T), \dots],$$

where T is the time-delay used for the reconstruction. d time-delayed vectors would be required to construct a d -dimensional space. For an unambiguous unfolding of the attractor, it is important to derive the embedding dimension d and the time delay T . This can be obtained using the false nearest neighbor and average mutual information calculations, respectively.

2. Average mutual information

In the absence of infinitely long data, it becomes important to calculate the optimum time delay. The prescriptions for choosing time delay are based on statistical information that is obtained from the time series. The autocorrelation function and average mutual information are two most commonly used criteria for choosing time delay.^{24,34} The first zero crossing of the autocorrelation function of the time series can be used as the optimum time delay; however, since autocorrelation is essentially a linear concept, it is not recommended for time series generated by a nonlinear process. A better criterion for the analysis of nonlinear time series comes from information theory. The idea is to evaluate the nonlinear dependence of time lagged variables based on mutual information shared between the variables. A comparison between autocorrelation function and average mutual information methods has been discussed by Fraser and Swinney.²⁵ The comparison illustrates why mutual information is

preferred for multi-dimensional phase portrait from single measurement. From the average mutual information function between time-lagged variables, the first minima of the function is chosen as the optimum time delay.

For obtaining average mutual information, individual probabilities $P(s(n)), P(s(n+T))$ and joint probabilities $P(s(n), s(n+T))$ were estimated from the time-delayed vectors by considering each time-delayed vector as an experiment. The values of pressure/intensity acquired at every sampling time interval would then be an event to be considered for calculating probabilities. Using these probabilities, one can then arrive at

$$I(T) = \sum_{i=1}^N P(s(n), s(n+T)) \log_2 \frac{P(s(n), s(n+T))}{P(s(n))P(s(n+T))}.$$

The quantity ($I(T)$), which is the average mutual information between the original time series and a delayed time series with a time delay of T , should be greater than equal to zero. The variation of $I(T)$ with time delay for all the time series discussed above is shown in Fig. 4. The top three curves in Fig. 4 are for periodic oscillations with rationally related frequencies, regions II, V, and VII (Fig. 2). The other curves belong to oscillations with either irrationally related frequencies or broadband frequencies, regions III, IV, and VI (Fig. 2). The optimal time delay for phase space reconstruction varies from 0.4 to 0.9 ms, in the various regions, as seen in Fig. 4.

3. False nearest neighbors

Phase space reconstruction is essentially a mapping of the original multivariate phase space, of dimensionality d_A to a subspace created from the time-delayed vector obtained from experiments, in a manner such that the invariants of the system remain constant. The dimension of the subspace, referred to as the embedding dimension, d_E , is one of the two important entities to be derived for a proper mapping or embedding, the second being the time-delay. A dimension equal to or larger than the embedding dimension can be used for phase space reconstruction but choosing a dimension lower than the embedding dimension will lead to false embedding. Appropriate embedding dimension can be calculated from the

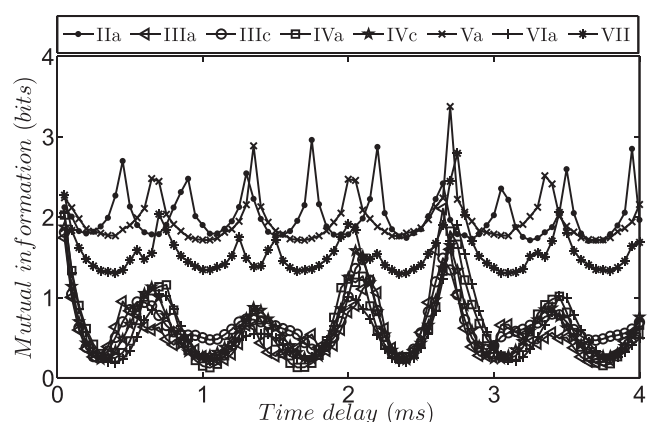


FIG. 4. Results for the calculation of optimum time-delay for phase space reconstruction using the average mutual information between time-delayed vectors from acquired time series.

measured times series using one of the several techniques available. A review of commonly used techniques such as singular-value decomposition of the sample covariance matrix, saturation with dimension of some system invariant, the method of false nearest neighbors, and the method of true vector fields is given by Abarbanel *et al.*²⁴

In the present study, the false nearest neighbor method, given by Kennel *et al.*,²⁶ is adopted, which determines the false crossings of the trajectory with itself, which may arise due to the projection of the system by a low dimensional space. The algorithm finds the percentage of false neighbors created due to false crossing of trajectories while increasing the embedding dimension. At an appropriate embedding dimension, the percentage of false nearest neighbors will go to zero. The subspace thus obtained has the correct dimension of the phase space, in order to unfold the phase space attractor without any ambiguity. A typical plot obtained for each of the cases discussed in the paper has been reported in Fig. 5. The trend of the variation of the percentage of false nearest neighbor estimates for different oscillations with respect to the embedding dimension, d_E , suggests $d_E = 5$ as an optimum embedding dimension since the percentage of false nearest neighbors for all the states vanishes at $d_E = 5$. Henceforth, quantitative information from phase space reconstruction of strange attractors has been derived using $d_E = 5$.

4. Reconstructed attractors

The three-dimensional phase portrait representations of the various states obtained in our system are arranged in the order of their occurrence in the bifurcation plot (Fig. 2) in Fig. 6, starting with the limit cycle. We find that the characteristics of simultaneously measured flame intensity time series data are similar to the pressure time series data (see Kabiraj *et al.*³²). For brevity, we have reported results based only on pressure time series data in this paper.

Limit cycle (Fig. 6(IIa)), as expected, is represented by a single loop in the phase space. But, the introduction of new frequencies due to the next bifurcation results in aperiodic oscillations and the loop turns into a dense toroidal structure, as can be seen in pressure oscillations (Figs. 6(IIIa) and 6(IIIb)). A toroidal structure in the phase space is an indication of quasi-periodic oscillations. Quasi-periodicity is also

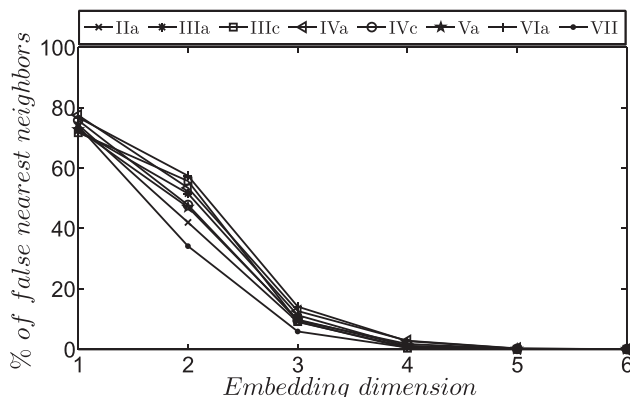


FIG. 5. Results for the calculation of the embedding dimension for phase space reconstruction using the false nearest neighbor method.

reflected in the power spectrum (Figs. 3(IIIb) and 3(IIId)) in the form of incommensurate frequency components (365.3 and 571.3 Hz). Due to the presence of incommensurate frequencies, the phase space trajectory evolves on the surface of a torus, never closing on itself. As we change the control parameter, within the quasi-periodic region (region III) in Fig. 2, there is a competition between the two major frequencies eventually leading to the introduction of a third incommensurate frequency (f_3 in Fig. 3(IVb)) causes the toroidal structure to become unstable and break down resulting in a strange attractor as seen in Fig. 6(IVa). This structure corresponds to the time series and the frequency spectrum that shows the presence of broadband frequency content in Fig. 3(IVb). Broadband frequency content and strange attractor hints towards the presence of chaotic oscillations.

To identify whether the obtained attractor (Fig. 6(IVa)) is a strange attractor (possesses an inherent dimension which is not an integer but rather a fraction), we evaluate the correlation dimension of the attractor using the Grassberger-Procaccia algorithm.²⁸ Subsequently, to find out if the oscillations are chaotic in nature, we calculate the maximal Lyapunov exponent using the algorithm suggested by Kantz.²⁹ These are discussed in the following paragraphs.

According to the Grassberger-Procaccia algorithm, the correlation dimension is obtained from the calculation of the correlation sum of all the points in the phase space. This correlation sum is given by

$$C(r) = \lim_{N \rightarrow \infty} \frac{1}{N^2} \left(\text{number of pairs of points } x_i, x_j \text{ with distances } s_{ij} < r \right),$$

where N is the total number of points, s_{ij} is a distance measure (here, taken as the Euclidean distance, in the phase space, between points x_i and x_j). As $r \rightarrow 0$, this function is found to have a power law dependence,

$$\lim_{r \rightarrow 0} C(r) \propto r^{d_c},$$

where d_c is an estimate of the correlation dimension of the attractor. In Figs. 7 and 8 the plot for $C(r)$ vs. r for the attractors, corresponding to regions IV and VI is given. It is seen that a scaling region where the power law dependence can be seen is found for r in the range $\sim 20 - 100$. Corresponding to these plots, the value of local slope with respect to r , for dimensions 6, 8, 10, and 12 have been given in Figs. 9 and 10. In the scaling region, the value of slopes gives an estimate of the correlation dimension of the particular attractor. For region IV, the value of slope in the scaling region fluctuates significantly. However, at high dimensions, it seems to have saturated. For region VI, slopes in the scaling region, calculated for different dimensions follow a more robust trend. For the two attractors in region IV and region VI, the correlation dimension, calculated from curves at dimension 12, is found to be 5.5 and 4.6, respectively. However, the scaling region used to estimate the correlation dimension for region IV (Fig. 9) is narrow compared to that obtained for region VI (Fig. 10).

Chaotic dynamics in a dynamical system is indicated by the presence of positive Lyapunov exponents. Lyapunov

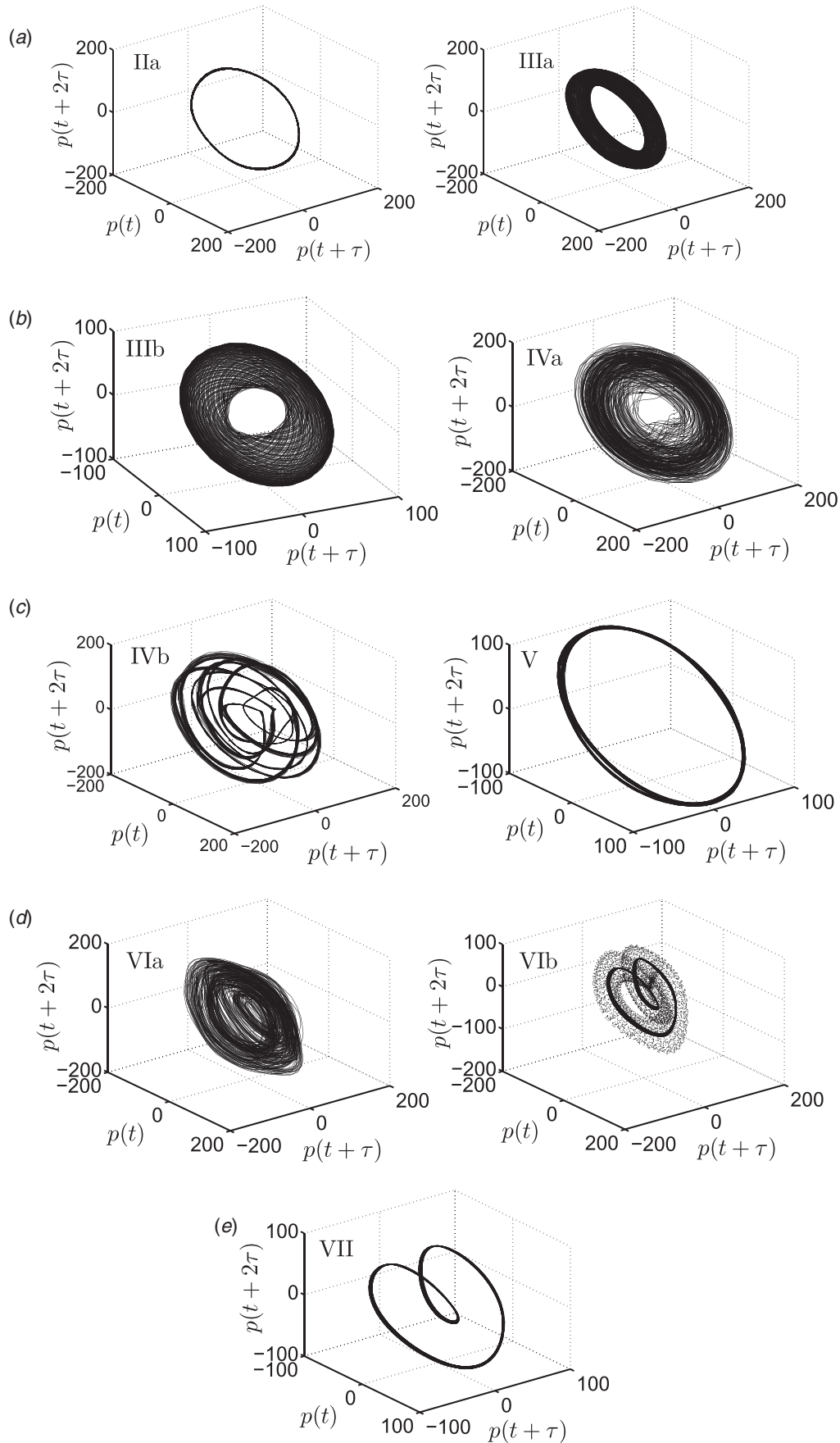


FIG. 6. Reconstructed phase portraits from measured pressure time series for different oscillation states, sequentially arranged in the order of their occurrence in the bifurcation diagram, Fig. 2. The labels are in accordance with the bifurcation plot.

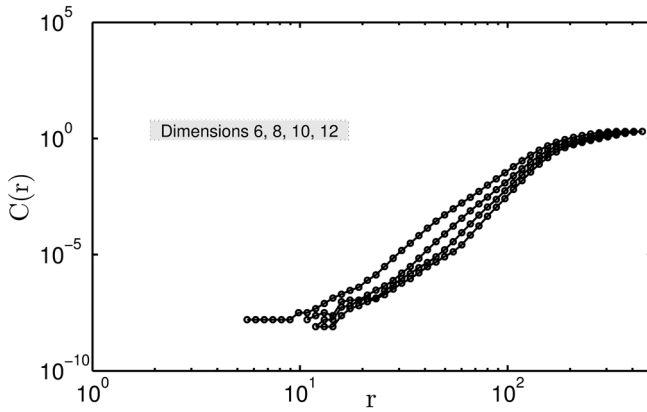


FIG. 7. Plot for the correlation sum for the attractor in region IV, Fig. 6(IVa). The variation with respect to r is plotted for dimensions 6, 8, 10, and 12. A data set with 16 000 points was considered for obtaining the plot.

exponents, by definition are a measure of the exponential divergence in time, of two neighboring phase space trajectories. A positive exponent implies that any uncertainty in estimation of the dynamical state of the system will grow exponentially in time. To identify the presence of chaotic dynamics in our system, we calculate the maximal Lyapunov exponent using the method given by Kantz.²⁹ According to the algorithm, one finds the average separation between neighboring trajectories in the reconstructed phase space as time evolves and the evolution in the average separation is searched for an exponential trend. More specifically, the average separation $S(\Delta n)$ is calculated as a function of temporal separation Δn

$$S(\Delta n) = \frac{1}{T} \sum_{t=1}^T \ln \left(\frac{1}{|\mathcal{U}_t|} \sum_{i \in \mathcal{U}_t} \text{dist}(x_t, x_i; \Delta n) \right),$$

where \mathcal{U}_t is the neighborhood of any point x_t in the phase space and $\text{dist}(x_t, x_i; \Delta n)$ is defined as

$$\text{dist}(x_t, x_i; \Delta n) = |x_{t+\Delta n} - x_{i+\Delta n}|.$$

The quantity $S(\Delta n)$ scales linearly with Δn in an intermediate range with a slope corresponding to the maximal Lyapu-

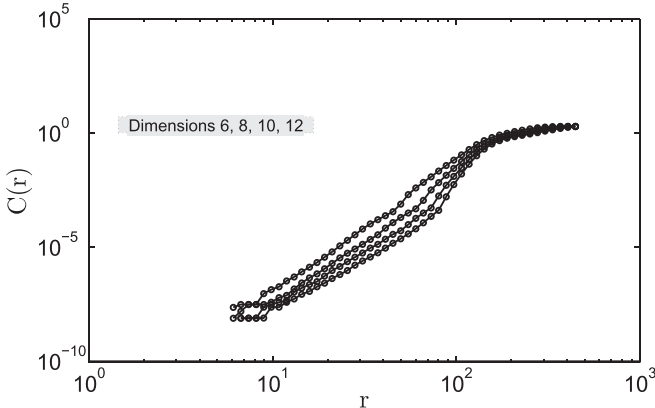


FIG. 8. Plot for the correlation sum for the attractor in region IV, Fig. 6(VIa). The variation with respect to r is plotted for dimensions 6, 8, 10, and 12. A data set with 16 000 points was considered for obtaining the plot.

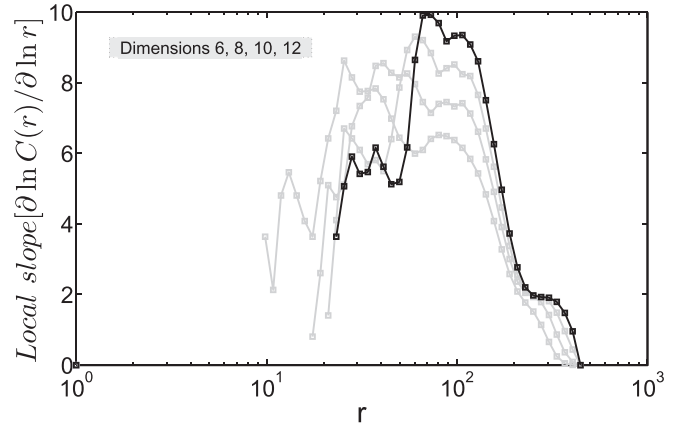


FIG. 9. Local slopes of the correlation sum in Fig. 7. The correlation dimension is evaluated from the curve corresponding to a dimension 12 (in black).

nov exponent. Further details about the algorithm and its implementation on experimentally acquired time series data can be found in Kantz,²⁹ Kantz and Schreiber.¹⁸

According to the bifurcation analysis of our system, regions IV and VI in the bifurcation plot are the possible chaotic states. In accordance with the Kantz algorithm, variation in $S(\Delta n)$ with Δn with an embedding dimension of 4, 6, 8, 10, and 12 for regions IV and VI is given in Figs. 11 and 12, respectively. The slope of a linear fit to the curves for embedding dimension 12, shown by the dashed line gives values 0.00041 and 0.00051 per time step. As data have been acquired with a sampling rate of 10 kHz, the maximal Lyapunov exponent corresponding to these slopes comes out to be 4.1 ± 1.4 and 5.1 ± 0.6 for region IV and region VI, respectively. The range of Δn to be searched for, to obtain the scaling region is quite large in both cases owing to the high sampling rate. In both cases, exponential divergence between neighboring trajectories occurs amidst a highly cyclic trend of the time series (number of cycles corresponding to a Δn of 1000 $O(10)$). The maximal Lyapunov exponent for both the regions is a positive value, indicating the chaotic nature of the system. Now that all the states have been characterized individually, we will discuss the entire bifurcation scenario.

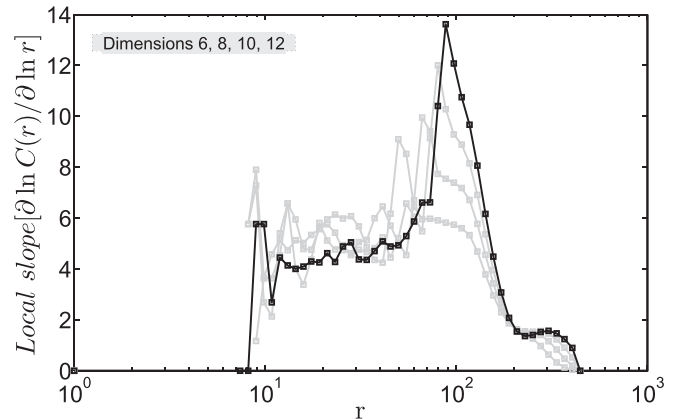


FIG. 10. Local slopes of the correlation sum in Fig. 9. The correlation dimension is evaluated from the curve corresponding to a dimension 12 (in black).

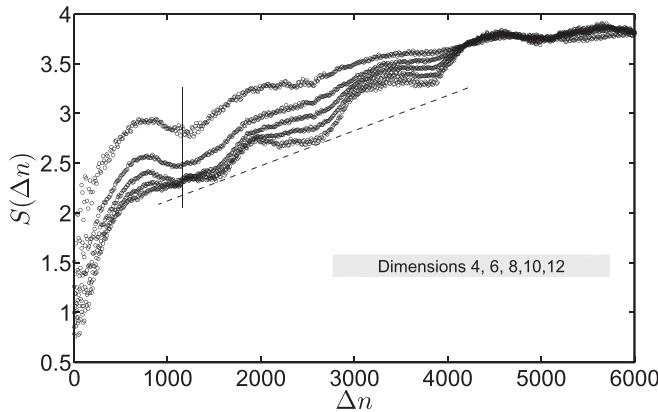


FIG. 11. Estimation of the maximal Lyapunov exponent (4.1 ± 1.4) (region IV) for dimensions 4, 6, 8, 10, and 12. A data set of 16 000 points was considered for calculations. The dashed line indicates a linear fit.

In our experiments, the quasi-periodic state is followed by chaotic oscillations. The system follows a torus breaking route to chaos starting from a limit cycle evolving into a two-frequency quasi-periodic state and eventually the two torus structure of the quasi-periodic attractor breaks down as a result of a third incommensurate frequency, thus leading to the emergence of a chaotic state. This torus breaking route to chaos is also called the Ruelle-Takens scenario.^{30,31,35} The strange attractor is then followed by periodic mode-locked oscillations featuring several rationally related frequencies (Fig. 3(IVd)). The phase space representation is given by Fig. 6(IVb). The structure is a closed loop which indicates a periodic nature of the oscillation, while following several turns before closing on itself which is because of the presence of a number of frequencies.

Following this state, the system once again enters a state with periodic oscillations given in Fig. 3(Va). The frequency spectrum (Fig. 3(Vb)) contains frequencies $f_2, f_2/2, f_2/4$ indicating this could be a period-4 state. The contribution from $f_2/2$ and $f_2/4$ being of very low order when compared to f_2 result in an attractor which consists of two very closely spaced loops in Fig. 6(Vb). This periodic state exists for a long range of control parameter before the next bifurcation which results in another aperiodic state.

Region (VI) exhibits chaotic oscillations resulting from a bifurcation of the periodic state. From the frequency spectrum, Fig. 3(VIb), and the reconstructed attractor, Fig. 6(VIa), it is observed that this could be another strange chaotic attractor. Figure 6(VIa) is a strange attractor, corresponding to the time series data obtained for $x_f = 33.9$ cm, and clearly shows the characteristics of the chaotic behavior observed in region (VI). The correlation dimension for this strange attractor is calculated to be 4.6 and the positive maximal Lyapunov exponent is 5.1 ± 0.6 . As discussed earlier, this state goes through an intermittent transition to period-2 oscillations.

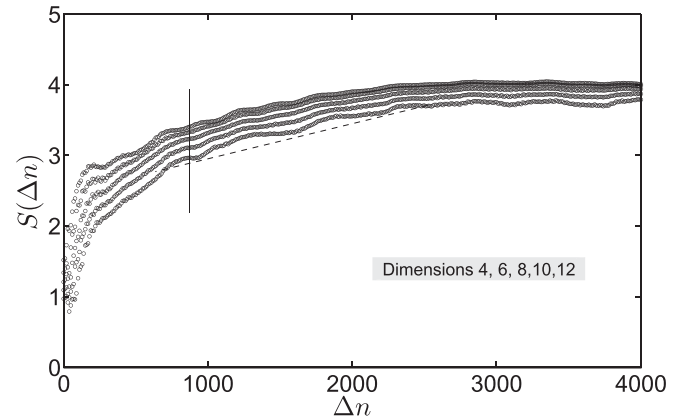
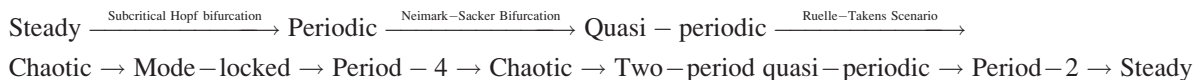


FIG. 12. Estimation of the maximal Lyapunov exponent (5.1 ± 0.6) (region VI) for dimensions 4, 6, 8, 10, and 12. A data set of 16 000 points was considered for calculations. The dashed line indicates a linear fit.

In the reconstructed phase space for pressure (Fig. 6(VIb)), we have shown phase space representation of the intermittent oscillations that alternate between period-two and a two-period quasi-periodic attractor. The dark loop is the period-two attractor which is embedded within a quasi-periodic attractor represented using light dotted markers in the reconstructed phase portrait. Once the flame location is changed, the system evolves to a period-two attractor via a very narrow window of stable quasi-periodic attractor. The window of this stable quasi-periodic oscillation is too insignificant to be labelled separately as another region. The phase space representation of the period-2 oscillations for region VII (Fig. 2) is shown in Fig. 6(VII). The system seems to follow a reverse quasi-periodic transition from chaotic to periodic oscillations. Region VIII (Fig. 2) is again the steady state (fixed point) to which the system eventually returns.

IV. DISCUSSIONS

We have presented an experimental bifurcation analysis conducted on a prototypical combustion driven thermoacoustic system. Changing the position of the combustion zone with respect to the duct causes the appearance of oscillations in the flames and in the acoustic pressure. This first bifurcation in the system is a subcritical Hopf bifurcation leading to limit cycle oscillations. However, the dynamics of thermoacoustic oscillations in combustion systems is not limited to limit cycle oscillations and although the system we study is a highly simplified version of a practical combustion system, variation of the flame location induces additional bifurcations. Bifurcation of limit cycle oscillations gives rise to quasi-periodic oscillations and changing the flame location further gives rise to chaotic oscillations. The sequence of bifurcations we observed in our experiments is summarised below



The sequence of bifurcations to chaotic oscillations, exhibited by the system is similar to the route to chaos in other physical systems, such as the Rayleigh-Bénard convection, popularly known as the quasi-periodic route to chaos or the Ruelle-Takens scenario. Transitions to complex oscillation states and the specific route to chaos observed in the present investigation arise from complex interactions between several processes; flame dynamics, acoustics, hydrodynamics, and heat transfer being the most significant processes. A strong coupling between these processes exists during the occurrence of combustion instability. However, it is still possible to shed light on the most likely cause of the presence of interesting system dynamics seen here, based on previous investigations that hint towards the importance of flame-acoustic interaction in combustion driven thermoacoustic systems.

The presence of combustion in an acoustic field, in particular the flame response to acoustic fluctuations, is known to be responsible for nonlinear aspects of thermoacoustic instability. A simplified analytical treatment of combustion instability (for instance, refer to the analysis by Dowling⁷) indicates that a nonlinear response of the flame to the incident acoustic fluctuations can explain nonlinear features such as the presence of limit cycles, subcritical bifurcation and triggering. This is further supported by the more recent describing function analysis¹⁶ of combustion instability, for a combustor similar to the present investigation. Complex nonlinear states in addition to limit cycle oscillations have also been reported, for instance by Jahnke and Culick,⁸ where quasi-periodic thermoacoustic oscillations were obtained in a dynamical system analysis using numerical continuation approach of thermoacoustic instability and by Sterling¹² in a numerical bifurcation analysis where a period doubling scenario was observed. Incorporation of nonlinear flame-acoustic interaction to explain the observed results in the analytical/numerical/experimental treatment of thermoacoustic instability is the common feature of the above mentioned studies.

Further, there is now a consensus in the combustion instability community that nonlinear gas dynamical processes are not significant in many premixed gas turbine combustors, where reported pressure amplitudes are typically on the order^{6,9,10} of $P'/\bar{P} \sim 1 - 5\%$ suggest that acoustic (i.e., gas dynamic) processes essentially remain in the linear regime, even under limit-cycle operation, and that it is the relationship between flow and heat release oscillations that provides the dominant nonlinear dynamics in premixed combustors. Therefore, in our combustor where $P'/\bar{P} \sim 0.1\%$, we can confidently rule out nonlinear gas dynamics as a cause of nonlinearity.

Based on the results summarized above and other previous investigations, we can surmise that a nonlinear flame response largely governs the behavior of thermoacoustic oscillations, including the bifurcations leading to chaos that have been observed in this report. Specifically in our experiments, changes in the flame location directly change the location of the combustion zone with respect to the acoustic field of the duct (standing wave). This in turn leads to changes in flame response and hence the overall dynamics of the self-excited heat release and pressure oscillations.

Flame surface area oscillation is the dominant mechanism generating unsteady heat release rate (cf., Schuller *et al.*¹⁷) in our experiments. The unsteady heat release rate gets coupled to pressure fluctuations during combustion instability. Changes in this flame-acoustic interaction at different oscillation states is reflected in pressure oscillations as well as in flame surface oscillations, as can be seen in high speed flame images (see Kabiraj *et al.*,³² Figs. 6–9).

In addition, it should also be noted that along with flame-acoustic interactions, other important processes, also contribute to the dynamics of oscillations. In practical combustion systems, complex fluid flow interactions¹¹ in the periphery of the confined combustion zone play a non-trivial role in determining the resulting thermoacoustic oscillations. Also important is the role of oscillatory heat transfer at the burner.²⁷ These processes are significant and need to be considered in detailed modeling approaches. However, concerning our experiments, these processes might not undergo changes at different flame locations and, therefore, do not participate in the bifurcation behavior. Hence, we speculate that, nonlinear flame-acoustic response turns out to be the most plausible mechanism responsible for the observed dynamics.

V. CONCLUSIONS

In this paper, we have seen that due to the nonlinear interactions between combustion and acoustics, a simple thermoacoustic system can exhibit a rich variety of dynamics. The nonlinear nature of thermoacoustic oscillations has been investigated from the point of view of dynamical systems theory. This approach enabled us to characterize and classify the behavior of the system in the linearly unstable regime. A variety of attractors—periodic, quasi-periodic, and chaotic states were observed in the system, as a control parameter was changed. A route to chaos for thermoacoustic oscillations is established experimentally for the first time. We show that, as the location of the heat source is gradually varied, self-excited periodic thermoacoustic oscillations undergo transition to chaos via the Ruelle-Takens scenario. Similar behavioral patterns in the oscillations have been observed to occur in several other nonlinear processes occurring in nature.

The phenomena observed in this study are related to the inherent nonlinear processes in combustion instability and, therefore, such dynamics is also expected to exist in practical systems. Accordingly, this information is quite critical and should be considered while constructing accurate models for thermoacoustic instability and designing effective control techniques. Practical combustion systems are highly susceptible to frequencies corresponding to the natural modes of structural components, which can cause resonance and can lead to catastrophic failure.^{33,36} For the case of quasi-periodic and mode-locked states, a number of frequencies will be present in the spectrum. During a chaotic state, the oscillations will be broadband in nature. As a consequence, resonant structural excitation is more likely to happen during the occurrence of states such as quasi-periodic, mode-locked, and chaotic oscillating than during the occurrence of limit cycle oscillations. Additionally, aperiodic behavior results in

variable amplitude pressure oscillations which can cause a higher fatigue loading, augmented crack formation, and propagation and therefore a higher wear and tear of the structural components constituting the combustor.³⁶ Consequently, the presence of nonlinear thermoacoustic oscillations can potentially reduce the performance and the life span of a combustor.

ACKNOWLEDGMENTS

This work was funded by the Department of Science and Technology, India. The authors gratefully acknowledge Mr. Joseph George for his critical suggestions.

- ¹M. Kitano, T. Yabuzaki, and T. Ogawa, *Phys. Rev. Lett.* **50**, 713–716 (1983).
- ²H. Gotoda, H. Nikimoto, T. Miyano, and S. Tachibana, *Chaos* **21**, 013124 (2011).
- ³H. Gotoda, T. Miyano, and I. G. Shepherd, *Phys. Rev. E* **81**, 026211 (2010).
- ⁴T. Yazaki, S. Takashima, and F. Mizutani, *Phys. Rev. Lett.* **58**, 1108–1111 (1987).
- ⁵T. C. Lieuwen and V. Yang, *Combustion Instabilities in Gas Turbine Engines: Operational Experience, Fundamental Mechanisms, and Modeling* (Progress in Astronautics and Aeronautics, AIAA, Inc., 2005).
- ⁶A. P. Dowling, *J. Fluid Mech.* **346**, 271–290 (1997).
- ⁷A. P. Dowling, *J. Fluid Mech.* **394**, 51–72 (1999).
- ⁸C. C. Jahnke and F. E. C. Culick, *J. Propul. Power* **10**, 508–517 (1994).
- ⁹A. A. Peracchio and W. M. Proscia, *J. Eng. Gas Turbines Power* **121**, 415–421 (1999).
- ¹⁰T. Lieuwen, *J. Propul. Power* **18**, 61–67 (1992).
- ¹¹K. C. Schadow and E. Gutmark, *Prog. Energy Combust. Sci.* **18**, 117–132 (1992).
- ¹²J. D. Sterling, *Combust. Sci. Technol.* **89**, 167–179 (1993).
- ¹³S. Lei and A. Turan, *Combust. Theory Modell.* **13**, 541–557 (2009).
- ¹⁴A. Fichera, C. Losenno, and A. Pagano, *Appl. Energy* **70**, 179–191 (2001).
- ¹⁵S. Candel, *Proc. Combust. Inst.* **29**, 1–12 (2002).
- ¹⁶N. Noiray, D. Durox, T. Schuller, and S. Candel, *J. Fluid Mech.* **615**, 139–167 (2008).
- ¹⁷T. Schuller, D. Durox, and S. Candel, *Combust. Flame* **134**, 21–34 (2003).
- ¹⁸H. Kantz and T. Schreiber, *Nonlinear Time Series Analysis* (Cambridge University Press, 2003).
- ¹⁹J. P. Gollub and S. V. Benson, *J. Fluid Mech.* **100**, 449–470 (1980).
- ²⁰Y. Matsui, *Combust. Flame* **43**, 199–209 (1981).
- ²¹P. J. Langhorne, *J. Fluid Mech.* **193**, 417–443 (1988).
- ²²S. H. Strogatz, *Nonlinear Dynamics and Chaos: With Applications to Physics, Biology, Chemistry, and Engineering* (Levant Books, 2007).
- ²³F. Takens, *Lect. Notes Math.* **898**, 366 (1981).
- ²⁴H. D. I. Abarbanel, R. Brown, J. J. Sidorowich, and L. S. Tsimring, *Rev. Mod. Phys.* **65**, 1331–1392 (1993).
- ²⁵A. M. Fraser and H. L. Swinney, *Phys. Rev. A* **33**, 1134–1140 (1986).
- ²⁶M. B. Kennel, R. Brown, and H. D. I. Abarbanel, *Phys. Rev. A* **45**, 3403–341 (1992).
- ²⁷H. J. Merk, *Appl. Sci. Res.* **8**, 1–27 (1958).
- ²⁸P. Grassberger and I. Procaccia, *Phys. Rev. Lett.* **50**, 346–349 (1954).
- ²⁹H. Kantz, *Phys. Lett. A* **185**, 77–87 (1994).
- ³⁰D. Ruelle and F. Takens, *Commun. Math. Phys.* **20**, 167–192 (1971).
- ³¹A. H. Nayfeh and B. Balachandran, *Applied Nonlinear Dynamics: Analytical, Computational, and Experimental Methods* (Wiley VCH, Weinheim, 2004).
- ³²L. Kabiraj, R. I. Sujith, and P. Wahi, *J. Eng. Gas Turbines Power* **134**, 031502 (2011).
- ³³R. Kurz and K. Brun, in *Proceeding of the Thirty Sixth Turbomachinery Symposium* (Texas A&M University, College Station, TX, 2007).
- ³⁴T. Schreiber, *Phys. Rev. E* **47**, 2401–2404 (1993).
- ³⁵R. C. Hilborn, *Chaos and Nonlinear Dynamics: An Introduction for Scientists and Engineers* (Oxford University Press, 2000).
- ³⁶S. Suresh, *Fatigue of Materials* (Cambridge University Press, 2000).